Coulomb collision model for use in nonthermal plasma simulation

Andrew M. Chap and Raymond J. Sedwick

Phys. Rev. E **95**, 063209 — Published 29 June 2017

DOI: 10.1103/PhysRevE.95.063209

Coulomb collision model for use in non-thermal plasma simulation

Andrew M. Chap* and Raymond J. Sedwick
Department of Aerospace Engineering, University of Maryland, 3146 Glenn L Martin Hall, College Park, MD 20740 USA
(Dated: June 8, 2017)

In kinetic simulations of non-Maxwellian plasmas, the calculation of particle scattering due to Coulomb collisions has no simple approximation. In such simulations, the number of collision interactions a particle experiences in a single time-step is typically too large for direct calculation. In this work, the cumulative effect of a series of binary collisions is calculated numerically in a stochastic manner, and heuristic trends are produced as functions of the local plasma parameters. The result is a collision model suitable for implementation into a kinetic plasma simulation. The presence of low-probability, high-angle scattering due to close collision encounters is defined and described, and this effect is demonstrated in a test problem simulation of weakly collisional counter-streaming ion beams.

I. INTRODUCTION

A. Plasma simulation overview

The velocity of a single charged particle in a population of other charged particles is affected by the Coulomb electric force between that particle and all other charged particles. In the simulation of charged particle plasmas, well-established methods for accounting for the Coulomb force include the following:

- The plasma fluid approximation [1] is suited for plasmas in which the particle velocities follow a Maxwell-Boltzmann distribution, the velocity of any one particle changes quickly relative to the time-scale of the plasma, and the spacing between particles is small in comparison to the length scale of the plasma. In this way, the bulk velocity and thermal velocity of each plasma species are well-distinguished.

- Poisson's equation, typically as part of a particle-in-cell approach [2] is effective at calculating the long-range force between particles by weighting these particles to a spatial grid, but the resolution of short-range forces is limited by both the magnitude of particle weighting as well as the resolution of the spatial grid.

- The N-body simulation method [3] is the truest method of calculating both short-range and long-range forces between particles, however the resolution is severely limited by particle weighting for systems in which the real particle count is high, and the treatment of boundary conditions in N-body simulations typically requires a separate approach.

* amchap@umd.edu

B. A cumulative Coulomb collision model

This work is focused on short-timescale changes in the velocities of charged particles in a non-thermal plasma. To this end, a single non-weighted charged particle (hereafter referred to as the "test particle") moving through a uniform population of non-weighted charged particles (hereafter referred to as the "field particles") is examined in order to develop an approximation for Coulomb scattering that can be applied to kinetic plasma simulations. The change in velocity angle of the test particle is referred to as a "scattering," and the probability distribution of such a scattering is dependent on the field particle density, the relative velocity between the test particle and field particle, and the amount of time over which the scattering occurs. In the development of the present method, it is assumed that there is no change in the density or the velocity distribution function of the field particles over the scattering time. It is also assumed that the center-of-mass frame stays constant over the scattering time, so that there is no energy exchange between the test particle and field particles. The energy exchange between the test particle and field particles is realized through the conversion from the center-of-mass frame to the laboratory frame.

For application to a particle-in-cell simulation, the present model may be implemented by randomly pairing macroparticles at each time step. In the center-of-mass frame of a pair, the first macroparticle is represented by the test particle and the second macroparticle by the field particles. The field particles are assumed to all have velocity equal to that of the second macroparticle, and density equal to the local density of the field particle species. After applying the present model to the first macroparticle (the test particle), the second macroparticle receives the reverse of same collision and in this way momentum and energy are conserved. If the simulation time-step is small compared to the time-scale of the plasma evolution, then collisions implemented this way will collectively model the collision-driven thermalization of the plasma.

This article is organized as follows:

- In Sec. II other collision models used for non-thermal plasma simulations are reviewed.
- In Sec. III the "cumulative binary collision approximation" is presented and a method for efficiently calculating a cumulative scattering angle from a large number of binary collisions without energy transfer is outlined. These calculations serve as the basis for which the heuristic model is later derived.
- In Sec. IV the validity of the cumulative binary collision approximation is evaluated by comparing its results to the results of N-body simulations of identical scenarios.
- In Sec. V heuristic formulae are presented for recreating the effect seen in Sec. III for a plasma simulation. This section contains the complete collision model that is the focus of this work.
- In Sec. VI results obtained from the present collision model are compared to those obtained by other collision models.
- In Sec. VII the collision model is implemented in a particle-in-cell simulation of a highly non-thermal, weakly collisional plasma and the results are compared to a true N-body simulation of an identical scenario.
- In Sec. VIII a discussion on low impact parameters is presented in the context of commonly used formulae for calculating a minimum impact parameter.

II. BACKGROUND

A. Previous work

A method for simulating Coulomb collisions of macroparticles was first proposed by Takizuka and Abe [4] and included details on a pair-matching Monte Carlo implementation, but no comparison to direct calculation of binary collisions was performed.

The effect of a series of binary collisions on a charged particle was first addressed by Nanbu [5] who used direct calculations of binary collisions to find the scattering angle distribution functions and created a collision model to replicate it. This work included an analytical derivation for the scattering angle to approximate the effect of low-angle collisions.

Dimits *et al.* [6] argued that Nanbu's binary collision method was identical to the Lorentz collision operator and assessed Nanbu's analytical model as such. However, both Nanbu and Dimits failed to identify the heavy tail of the probability distribution of the scattering angle that is clearly present from the results of Nanbu's data from simulating a series of binary collisions. Additionally, none of the referenced works offer an analysis of the validity of simulating a cumulative Coulomb scatter as a series of binary collisions.

Rutherford's famous discovery of the nucleus [7] involved a derivation of the probability distribution for high-angle scattering of light ions off of gold nuclei. Conte [8] applied this formula to counter-streaming charged particle beams and used it to calculate beam particle loss due to high-angle Coulomb collisions but did not apply it to cumulative low-angle scatters.

B. The present work

The present work seeks to identify both the cumulative effect of many small-angle scatters as well as the effect of a single high-angle scatter and to recover both in a piecewise continuous heuristic model. This work is the first to identify that the probability distribution of a cumulative Coulomb scattering angle Θ transitions from an exponential form $f_\Theta(\theta) \sim \exp(-\theta^2)$ to a power-law form $f_\Theta(\theta) \sim \theta^{-3}$ as θ increases. Additionally, the present work differs from previous works in that the model is based entirely on the results of numerical experiments, rather than relying on the Coulomb logarithm which is not well defined for highly non-thermal and non-neutral plasmas. Like previous models, this model uses the assumption that when the distance between two particles is large, they can be considered to have no interaction at all. The cutoff distance at which this assumption is applied is denoted as $b_{\max}$ and physically symbolizes either the distance at which space charge is accounted for via another calcuation such as Poisson's equation [2], or the distance at which Debye screening [9] is significant. The present work also benefits from the general advancements in computing that have taken place in the twenty years since the publication of Nanbu's work. At the time of Nanbu's publication, the computational resources required to calculate the number binary collision calculations used in the present work were simply not available. Despite this, Nanbu's model is still used in contemporary charged particle simulation [10] though it is the aim of this work to present a more accurate model.

C. Motivation for the present work

This work is motivated by the need for accurate simulation of Inertial Electrostatic Confinement (IEC) fusion [11], in which the fusion core typically consists of a highly non-thermal population of counter-streaming ion beams. In particular, in such IEC iterations as the Multiple Grid IEC [12, 13] or the Continuous Grid IEC [14], high-angle collisions may play an important role in ion loss rates as well as the sole mechanism for the transfer of ions between beams intersecting at an angle. Additionally, a model which does not rely on an estimation of the Coulomb logarithm is beneficial for simulations in which the Coulomb logarithm can not be prudently applied.

III. THE CUMULATIVE BINARY COLLISION APPROXIMATION

A test particle of species α traveling through a field of N randomly positioned charged particles of species β will have its velocity vector changed by some angle Θ after an amount of time τ. The interactions that cause this change in angle may be approximated as the cumulative effect of independent binary collisions between the test particle and each field particle. The angle of scatter for a Coulomb collision between the test particle and a single field particle in the center-of-mass frame is [7]:

$$\theta = 2\tan^{-1}\left(\frac{q_\alpha q_\beta}{4\pi\epsilon_0\mu_{\alpha\beta}v_{\alpha\beta}^2 b}\right) \tag{1}$$

where q_α and q_β are the particle charges, $\mu_{\alpha\beta} \equiv (m_\alpha^{-1} + m_\beta^{-1})^{-1}$ is the reduced mass, $v_{\alpha\beta} \equiv |\mathbf{v}_\alpha - \mathbf{v}_\beta|$ is the relative speed between the particles, and b is the impact parameter (the perpendicular distance between the initial paths of the two particles in the center-of-mass frame). Because a collision model is typically only applied over a local region, only field particles with impact parameters $b < b_{\max}$ are considered. Over an amount of time τ of a particle simulation (usually equal to the simulation time-step), a particle of species α moving at a velocity $v_{\alpha\beta}$ relative to a population of particles of density n_β, will undergo a number of binary Coulomb collisions approximately equal to

$$N = n_\beta v_{\alpha\beta}\tau\pi b_{\max}^2 \tag{2}$$

which is the field particle density n_β multiplied by the volume of a cylinder with radius $b_{\max}$ and length equal to the relative distance the test particle travels over time τ.

The following derivation is similar to the derivation given in the appendix of Ref. 5. Let the initial velocity of a test particle be aligned with the z-axis, and let the axis rest in the center-of-mass frame of a single test particle/field-particle pair. The final velocity after N binary collisions will have a final scattering angle of Θ with respect to the z-axis. Because of the azimuthal symmetry of the problem, the final azimuthal angle is uniformly distributed between 0 and 2π. Let θ_i be the angle of the velocity vector before the i^{th} collision, $[\Delta\theta]_i$ be the change in the angle of the velocity vector due to the i^{th} collision given by Eq. (1), and $[\Delta\phi]_i$ be the azimuthal angle of this change, randomly selected between 0 and 2π. The azimuthal angle before the i^{th} collision, ϕ_i, has no effect on the final probability distribution function and so may be chosen to equal zero for the purpose of this derivation. The velocity vector after the i^{th} collision is found by rotating $\hat{\mathbf{z}}$ about the y-axis by $[\Delta\theta]_i$, then rotating the resultant vector about the z-axis by $[\Delta\phi]_i$ and lastly rotating that result about the y-axis by θ_i to effectively give $\hat{\mathbf{z}}$ the correct "starting position". In summary, the new velocity vector after the i^{th} collision is

$$\begin{aligned}\hat{\mathbf{v}}_{i+1} = &\begin{bmatrix}\cos(\theta_i) & 0 & \sin(\theta_i)\\ 0 & 1 & 0\\ -\sin(\theta_i) & 0 & \cos(\theta_i)\end{bmatrix}\\ &\times\begin{bmatrix}\cos([\Delta\phi]_i) & -\sin([\Delta\phi]_i) & 0\\ \sin([\Delta\phi]_i) & \cos([\Delta\phi]_i) & 0\\ 0 & 0 & 1\end{bmatrix}\\ &\times\begin{bmatrix}\cos([\Delta\theta]_i) & 0 & \sin([\Delta\theta]_i)\\ 0 & 1 & 0\\ -\sin([\Delta\theta]_i) & 0 & \cos([\Delta\theta]_i)\end{bmatrix}\hat{\mathbf{z}}.\end{aligned} \tag{3}$$

At this point, the derivation diverges from that of Ref. 5. The z-component of $\hat{\mathbf{v}}_{i+1}$ is equal to $\cos(\theta_{i+1})$, and so the new angle is found by evaluation of the z-component of Eq. (3):

$$\begin{aligned}\cos(\theta_{i+1}) =&\cos(\theta_i)\cos([\Delta\theta]_i)\\ &+\sin(\theta_i)\sin([\Delta\theta]_i)\cos([\Delta\phi]_i).\end{aligned} \tag{4}$$

To randomly distribute the field particles uniformly in a cylinder of radius $b_{\max}$, the impact parameter of each particle is calculated as $b_i = b_{\max}\sqrt{U_i}$ where each U_i is independently and uniformly distributed in $(0, 1)$ and so the angle of scatter from Eq. (1) becomes

$$[\Delta\theta]_i = 2\tan^{-1}\left(\frac{a}{\sqrt{U_i}}\right) \tag{5}$$

with the dimensionless parameter a introduced as

$$a \equiv \frac{q_\alpha q_\beta}{4\pi\epsilon_0\mu_{\alpha\beta}v_{\alpha\beta}^2 b_{\max}}. \tag{6}$$

The azimuthal angle is equally likely to take any value between 0 and 2π and so is calculated as

$$[\Delta\phi]_i = 2\pi V_i \tag{7}$$

where each V_i is independently and uniformly distributed in $(0, 1)$. Combining Eqs. (4), (5) and (7), and making the definition $C_i \equiv \cos(\theta_i)$, the recursive relation is

$$\begin{aligned}C_{i+1} = &\frac{U_i - a^2}{U_i + a^2}C_i\\ &+\frac{2a\sqrt{U_i}}{U_i + a^2}\sqrt{1 - C_i^2}\sin(2\pi V_i)\end{aligned} \tag{8}$$

where $C_0 = 1$ and the final cumulative scattering angle is $\Theta \equiv \cos^{-1}(C_N)$. In this formulation, the probability distribution of Θ is dependent only on the dimensionless variables a and N (defined in Eqs. (6) and (2) respectively). Eq. (8) is used for generating numerical data for cases in which a is large enough that evaluation of $U_i + a^2$ is not limited by machine precision.

A. The limit for small a

For small values of a, the evaluation of $U_i + a^2$ in floating point arithmetic may result in significant error. It is found that $a \lesssim 10^{-6}$ generates noticeable error in the evaluation of Eq. (8) in double-precision floating-point format. Taking the limit as $a \to 0$, Eq. (5) becomes

$$\lim_{a\to 0}[\Delta\theta]_i = \frac{2a}{\sqrt{U_i}}. \tag{9}$$

With Eq. (7) unchanged by this limit, the scattering is now equivalent to a random walk in a 2D plane with step length $2a/\sqrt{U_i}$. By separating this 2D walk into the x and y components of the now flat θ-plane, the final scattering angle can be expressed as the magnitude of the summation of each component:

$$\lim_{a\to 0}\Theta = 2a\sqrt{\left(\sum_{i=1}^{N}\frac{\cos(2\pi V_i)}{\sqrt{U_i}}\right)^2 + \left(\sum_{i=1}^{N}\frac{\sin(2\pi V_i)}{\sqrt{U_i}}\right)^2}. \tag{10}$$

The scattering angle in the $a \to 0$ regime now scales linearly with a, though the dependence on N remains non-trivial. To avoid calculating scattering angles greater than π, Eq. (10) can be replaced with

$$\lim_{a\to 0}\Theta = 2\tan^{-1}\left[a\sqrt{\left(\sum_{i=1}^{N}\frac{\cos(2\pi V_i)}{\sqrt{U_i}}\right)^2 + \left(\sum_{i=1}^{N}\frac{\sin(2\pi V_i)}{\sqrt{U_i}}\right)^2}\right] \tag{11}$$

which reduces to Eq. (5) for $N = 1$ but avoids the machine precision limitation inherent in Eq. (8) for small values of a.

IV. THE VALIDITY OF THE CUMULATIVE BINARY COLLISION APPROXIMATION

The validity of equation Eq. (8) in calculating the angle of the change in velocity of a particle over a time-step is examined by comparing it to an N-body simulation using identical parameters. For this validation to remain numerically tractable, the field particles are held in fixed locations ($m_\beta = \infty$, $v_\beta = 0$, $v_{\alpha\beta} = v_\alpha$). The field particles are randomly and uniformly distributed throughout a sphere of radius R at a density of n_β and the test particle starts at the sphere center moving with an initial velocity of $\mathbf{v}_\alpha$ parallel to the z-axis. At each time-step the test particle is accelerated only by those field particles that lie within a distance $b_{\max}$ of the test particle. To ensure that the simulated domain is large enough to keep the $b_{\max}$ sphere fully populated at all times, the radius of the simulation domain is $R = v_\alpha\tau + b_{\max}$ so that $\tilde{N} = n_\beta\frac{4}{3}\pi R^3$ field particles must be generated. A diagram of this method is shown in Fig. 1.

The N-body method used here is similar to that used in previous research [14] which is in turn based on the work of Aarseth [3]. The test particle trajectory is calculated using the following steps starting with $t_0 = 0$ and repeating until $t_k = \tau$ (where $t_k \equiv \sum_{k'=0}^{k}[\Delta t]_{k'}$):

1. Advance the position of the test particle over the first half of the time-step:

$$\mathbf{x}_\alpha(t_{k+1/2}) = \mathbf{x}_\alpha(t) + \mathbf{v}_\alpha(t)[\Delta t]_k/2. \tag{12}$$

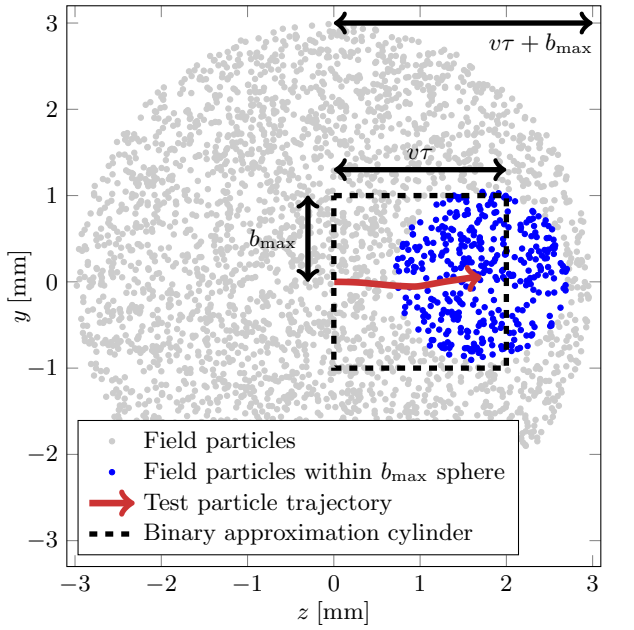

FIG. 1. A 2-dimensional cross-sectional schematic of the N-body simulation for testing the cumulative binary collision approximation. The test particle travels a distance of $v\tau = 2$ mm through a sphere of field particles but only experiences a force from field particles within a distance of $b_{\max} = 1$ mm.

2. For each i of $\tilde{N}$ field particles, find if it lies within a sphere of radius $b_{\max}$ centered on the test particle:

$$\mathbf{1}_{\alpha\beta,i} = [|\mathbf{x}_{\alpha\beta,i}| < b_{\max}] \tag{13}$$

where $\mathbf{x}_{\alpha\beta,i} \equiv \mathbf{x}_\alpha(t_{k+1/2}) - \mathbf{x}_{\beta,i}$.

3. Calculate the acceleration of the test particle due to the force from all field particles within the sphere

of radius $b_{\max}$:

$$\mathbf{a}_\alpha(t_{k+1/2}) = \frac{q_\alpha q_\beta}{4\pi\epsilon_0 m_\alpha} \sum_{i=1}^{\tilde{N}} \mathbf{1}_{\alpha\beta,i} \frac{\mathbf{x}_{\alpha\beta,i}}{|\mathbf{x}_{\alpha\beta,i}|^3}. \tag{14}$$

4. Advance the velocity of the test particle over the full time-step:

$$\mathbf{v}_\alpha(t_{k+1}) = \mathbf{v}_\alpha(t) + \mathbf{a}_\alpha(t_{k+1/2})[\Delta t]_k. \tag{15}$$

5. Advance the position of the test particle over the second half of the time-step:

$$\mathbf{x}_\alpha(t_{k+1}) = \mathbf{x}_\alpha(t_{k+1/2}) + \mathbf{v}_\alpha(t_{k+1})[\Delta t]_k/2. \tag{16}$$

6. Calculate the value of the next time-step using the minimum of a method of Aarseth [3] or a maximum time-step:

$$[\Delta t]_{k+1} = \min\left([\Delta t]_{\max}, \sqrt{\eta_1}\frac{|\mathbf{a}_\alpha(t_{k+1/2})|}{|\dot{\mathbf{a}}_\alpha(t_k)|}\right) \tag{17}$$

where $\dot{\mathbf{a}}_\alpha(t_k) = \left(\mathbf{a}_\alpha(t_{k+1/2}) - \mathbf{a}_\alpha(t_{k-1/2})\right)/[\Delta t]_k$ and the maximum allowed time-step is $[\Delta t]_{\max} = \eta_2/(n_\beta^{1/3} v_\alpha)$. η_1 and η_2 are chosen such that further decreasing either value does not significantly change the results of the simulation.

When $t_k = \tau$ the simulation stops and the cumulative scattering angle Θ_i is recorded as the angle between the initial velocity and the final velocity of the test particle. This process is repeated M times for a set of input parameters, where M is chosen such that the probability distribution function $f_\Theta(\theta)$ is smooth enough for confident comparison with other probability distribution functions.

Typically in a particle simulation, the time-step will be held to such a value such that $\tau < Cd/v$, where C is the Courant number [15], and the distance d is either the distance between grid points or the Debye length. For these cases, the distance a particle travels in a given time-step τ will almost always be less than the value $b_{\max}$, so tests of this method need not explore the parameter space where $b_{\max} \ll v_{\alpha\beta}\tau$. The probability distributions of the scattering angles for different values of $b_{\max}$ with constant values $v_\alpha = 10^3\,\mathrm{m/s}$, $\tau = 1\,\mu\mathrm{s}$, $n_\beta = 10^{11}\,\mathrm{m}^{-3}$, and $m_\alpha = 1\,\mathrm{AMU}$ are shown in Fig. 2. For the maximum value of $b_{\max} = 9.44\,\mathrm{mm}$, the number of field particles present in the N-body simulation is on the order of $\tilde{N} \approx 10^{13}$ and the number of field particles interacted with at any one time is on the order of $N \approx 10^{12}$. Using $\eta_2 = 0.05$, the number of time-steps for each test-particle trial is approximately 100 (increasing significantly in the rare case of near-collision.) The number of trials performed for each value of $b_{\max}$ was $M = 10^5$ for the N-body simulation (Fig. 2(a)) and $M = 10^7$ for the cumulative binary collision approximation (Fig. 2(b)).

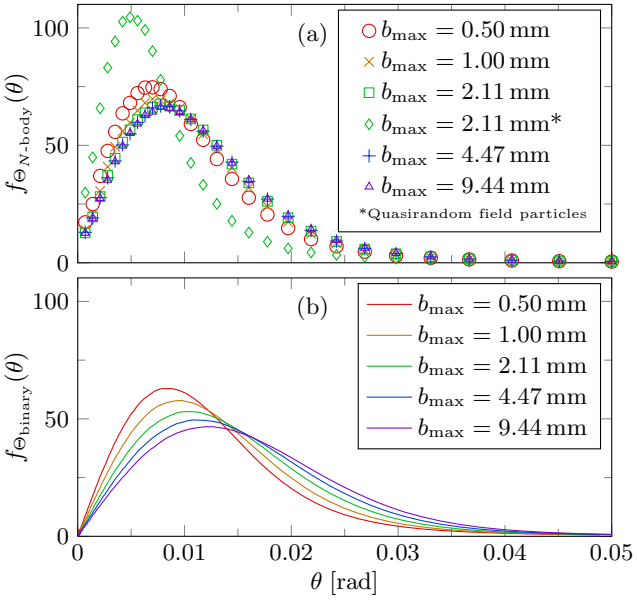

FIG. 2. Probability distribution functions for varying values of $b_{\max}$ for (a) results of the N-body simulation with fixed field particles and (b) results of the cumulative binary collision approximation.

A. Shortcomings of the cumulative binary collision approximation

The cumulative binary collision approximation tends to overestimate scattering angles because it assumes a complete collision between the test particle and all field particles. But if the assumption is that particle interactions should be neglected at distances greater than $b_{\max}$, field particles with an impact parameter b close to the value of $b_{\max}$ will only impart a partial collision to the test particle and so the effect of long-range Coulomb collisions becomes lessened.

Another shortcoming of the cumulative binary collision approximation is that it assumes a random distribution of field particles, but in an actual plasma, particles are not randomly distributed. The randomness of particle positions has been studied in the field of strongly coupled plasmas [16] whereby N-body (generally referred to in this field as "molecular dynamics") simulations are used to find the pair correlation function as a function of the single-species plasma coupling parameter: $\Gamma \propto n^{1/3}T^{-1}$. At low values of Γ, the particle velocities are high relative to the interparticle distance and the acceleration experienced by the particle due to the Coulomb interaction, so that the instantaneous positions of particles may be indistinguishable from a truly random distribution. At high values of Γ, the particles of the system are organized in a low-energy state and so the particle positions are distinguished from that of a random distribution. To test the effect of the randomness of field particle positions on the scattering angle, the same N-body test was performed with field particles positioned using

MATLAB's *haltonset* function [17] to uniformly fill the test volume with a quasi-random distribution (representative of a high value of Γ compared to that of a random distribution). It was found that this uniformity had a significant effect on shifting the peak of the probability distribution to a lower angle, while the high-angle portion of the distribution remained unchanged. The probability distribution of the scattering angle from this test are also shown in Fig. 2(a). A more thorough study of the relation between the coupling parameter of the field particles and the probability distribution of the scattering angle would require an efficient method of generating a random distribution of points with a specified value Γ. Another option could be to modify the cumulative binary collision approximation by adjusting the Coulomb force so that the magnitude is decreased when the interaction distance approaches the screening distance in a manner that is more accurate than simply applying a cutoff distance [18, 19]. However, for the remainder of this work it is assumed that Γ is small such that the distribution of particle positions of a single species is random.

Finally, it can be noted that the cumulative binary collision approximation has only two degrees of freedom, a and N, while the N-body fixed field particle simulation has three: a, N, and a third quantity: $n_\beta b_{\max}^3$, which scales as the number of particles within a sphere of radius $b_{\max}$. Because of the higher computational cost of the N-body fixed particle simulation as well as the additional degree of freedom it requires, the remainder of this article uses the cumulative binary collision approximation, in spite of its shortcomings, as a baseline for which to compare the formulated heuristics of the collision model that follows.

V. HEURISTIC FORMULAE FOR THE CUMULATIVE SCATTERING ANGLE

With the assumption that the cumulative binary collision approximation can be made, calculations are feasible enough such that the probability distribution function of Θ can be found over a range of a and N (from Eqs. (6) and (2)). The collision model outlined in this section takes a single random number input U, uniformly distributed on $(0, 1)$, and produces a scattering angle output with a probability distribution function that approximates that of the cumulative binary collision approximation. The convention has been chosen so that decreasing (increasing) the random number input results in an increasing (decreasing) of the output scattering angle. Though at times counterintuitive, this convention is preferable both for plotting purposes and because the randomly generated numbers have finer resolution when closer to zero [20].

A. Functional fits for numerical data

The present work has identified three regions of behavior based on the scattering angle after a large number of Coulomb collisions:

- The high-probability **low-angle region** is the collective effect of all scattering events over the time-step. It contains the angle of highest probability and is described by an exponential function.
- The low-probability, **high-angle region** is the result of the effect of one high-angle collision that is large in magnitude compared to all other scatters in that time-step. This region is well described by the analytically-determined probability distribution function for the closest expected Coulomb collision. In other words, it is the result of a single collision so large that all other collisions over the time-step are negligible.
- The mid-range **transition region** bridges the low-angle region with the high-angle region. It is best described by a linear fit of the logarithms of the variables involved, resulting in a power law.

For a single binary Coulomb collision, the cumulative distribution function of the scattering angle, or the probability that the resulting angle Θ will be greater than or equal to θ, ($F_\Theta(\theta) \equiv P(\Theta \geq \theta)$) is found in a straightforward manner from Eq. (5) by recognizing that U_1 is identical to $1 - F_{\Theta,\, N=1}$:

$$F_{\Theta,\, N=1}(\theta) = \begin{cases} 0 & \theta < 2\tan^{-1}(a) \\ 1 - \frac{a^2}{\tan^2\left(\frac{\theta}{2}\right)} & \theta \geq 2\tan^{-1}(a) \end{cases}. \tag{18}$$

Eq. (18) is suitable for the $N = 1$ case, but for large N there is no analytical solution, and so a heuristic model is formulated instead.

1. *High-angle region*

The high-angle region is found to be well described by choosing a dummy value of $b_{\max}$ such that $N = 1$ in Eq. (2), i.e. $\tilde{b}_{\max} \equiv (nv\tau\pi)^{-1/2} = b_{\max}/\sqrt{N}$. A dummy version of a is defined using Eq. (6) with $\tilde{b}_{\max}$ in place of $b_{\max}$: $\tilde{a} \equiv a\sqrt{N}$. The high-angle region of the cumulative distribution function then follows from Eq. (18) and results in

$$F_{\Theta,\text{high}}(\theta) = 1 - \frac{a^2 N}{\tan^2\left(\frac{\theta}{2}\right)}. \tag{19}$$

Note that $b_{\max}$ is not present in the term $a^2 N$. The probability distribution function $f_\Theta(\theta) \equiv \frac{d}{d\theta} F_\Theta(\theta)$ for the high angle region is

$$f_{\Theta,\text{high}}(\theta) = \frac{a^2 N}{\sin^2\left(\frac{\theta}{2}\right)\tan\left(\frac{\theta}{2}\right)} \tag{20}$$

which is equivalent to Eq. (2) in Ref. 7 (known as Rutherford Scattering). It is important to note that this equation demonstrates that the probability distribution of the scattering angle is a heavy-tailed distribution, and that any collision model that produces only an exponential probability distribution of scattering angles will tend to drastically underestimate the frequency of high-angle collisions. Inclusion of Eq. (20) in a collision model ensures that the collision model accurately produces high-angle scatters with the correct probability.

The continuous independent variable $u \in (0,1)$ is introduced as the domain of possible values of the discrete random number input U. With this convention it follows that $u \equiv 1 - F_\Theta(\theta)$ and so $\theta(u)$ for the high-angle region is found from Eq. (19) and is quite similar to Eq. (5):

$$\theta_{\text{high}}(u) = 2\tan^{-1}\left(\frac{a\sqrt{N}}{\sqrt{u}}\right). \tag{21}$$

2. Low-angle region

The low angle region is described by the work of Nanbu [5] and modified here to include a newly defined constant κ (dependent on a and N) which is less than unity to account for the fact that this region is not independently normalized. Additionally, a constant σ is used which corresponds to the most probable scattering angle, i.e. the maximum value of $f_\Theta(\theta)$, and scales generally as $a/\sqrt{N}$, but asymptotes to a value of $\pi/2$ when the effects of collisions approach isotropy (high a and/or high N). Using the formulation of Nanbu as a starting point, the probability distribution function of the low-angle region is found to be well-described by

$$f_{\Theta,\,\text{low}}(\theta) = \kappa\frac{\varsigma\sin(\theta)\exp\left(\varsigma\cos(\theta)\right)}{2\sinh(\varsigma)} \tag{22}$$

where $\varsigma \equiv \cos(\sigma)/\sin^2(\sigma)$. The cumulative distribution function can be found by integrating the probability distribution function of Eq. (22), i.e. $F_\Theta(\theta) \equiv \int_0^\theta f_\Theta(\theta')d\theta'$:

$$F_{\Theta,\,\text{low}}(\theta) = \kappa\left[1 - \frac{\exp\left(\varsigma\cos(\theta)\right) - \exp\left(-\varsigma\right)}{2\sinh(\varsigma)}\right] \tag{23}$$

and the scattering angle as a function of u is

$$\theta_{\text{low}}(u) = \cos^{-1}\left\{\frac{1}{\varsigma}\log\left[\exp(-\varsigma) + 2\sinh(\varsigma)\left(\frac{u-1}{\kappa} + 1\right)\right]\right\}. \tag{24}$$

For values of $\varsigma \gtrsim 100$ the evaluation of Eq. (24) results in exponential overflow, so the following can be used for these cases:

$$\theta_{\text{low},\,\varsigma>100}(u) = \cos^{-1}\left\{1 + \frac{1}{\varsigma}\log\left(\frac{u-1}{\kappa} + 1\right)\right\}. \tag{25}$$

3. Transition region

In between the low-angle and high-angle regions is a transition region that is not easily defined but is continuously monotonic. The transition region is chosen to be a linear fit in logarithmic space that minimizes the error when compared to the cumulative binary collision approximation. The bounds of the transition region are defined as u_{low} and u_{high}. The transition region is chosen to be a linear fit of the logarithms of θ and u, i.e. a power law. The chosen fit is

$$\theta_{\text{transition}}(u) = \theta_{\text{low}}(u_{\text{low}})\left[\frac{u}{u_{\text{low}}}\right] \wedge \left[\frac{\log\left\{\frac{\theta_{\text{low}}(u_{\text{low}})}{\theta_{\text{high}}(u_{\text{high}})}\right\}}{\log\left(\frac{u_{\text{low}}}{u_{\text{high}}}\right)}\right]. \tag{26}$$

B. Scattering angle as a function of a random seed

A piecewise function is created from Eqs. (21), (24) (or (25)), and (26):

$$\theta_{\text{Chap}}(u) = \begin{cases} \theta_{\text{high}}(u) & u < u_{\text{high}} \\ \theta_{\text{transition}}(u) & u_{\text{high}} < u < u_{\text{low}} \\ \theta_{\text{low}}(u) & u > u_{\text{low}} \end{cases}. \tag{27}$$

A single scattering angle is calculated from a single random number input U in the present model as $\Theta = \theta_{\text{Chap}}(U)$.

C. A comparison of function fits with numerical data

Numerical data is produced using Eq. (8). All calculations are performed in MATLAB and executed in parallel on an NVIDIA Tesla c2070 in double-precision floating-point format, which performs at an effective rate of approximately 1 nanosecond per binary collision evaluation including random number generation. M trials are performed, and in each trial, Eq. (8) is evaluated N times.

The result is a collection of independently produced values Θ_i, $i = 1 \ldots M$. The cumulative distribution function from these trials is

$$F_\Theta(\theta) = \frac{1}{M} \sum_{i=1}^{M} \mathbf{1}_{\Theta_i \leq \theta}. \tag{28}$$

Defining $\tilde{\Theta}$ as an ordering of Θ such that $\tilde{\Theta}_1 \geq \tilde{\Theta}_2 \geq ... \geq \tilde{\Theta}_M$, a function that relates a random number input to a scattering angle in a manner that replicates the numerical cumulative distribution function Eq. (28) is

$$\theta_{\text{binary}}(u) = \tilde{\Theta}_{\lceil M\, u \rceil} \tag{29}$$

where $\lceil \cdot \rceil$ is the ceiling function. These functions imply a probability of $1/M$ for each Θ_i. By choosing the constants σ, κ, u_{low}, and u_{high} such that the error is minimized between Eq. (29) and Eq. (27), then the scattering angles produced by Eq. (27) will have similar probability distributions to those produced by N evaluations of Eq. (4). The cost function for the optimization of the fit function is

$$C = \sum_{i=1}^{M} \left[\tilde{\Theta}_i - \theta_{\text{Chap}}\left(\tfrac{i-1/2}{M}\right) \right]^2. \tag{30}$$

By adjusting the values of σ, κ, u_{low}, and u_{high} so that the cost function is minimized, Eq. (27) becomes a good approximation for Eq. (29).

For the values of $a = 10^{-3}$ and $N = 10^3$, and using $M = 10^7$, the resulting plot of $\theta_{\text{binary}}(u)$ (smoothed for clarity) is shown in Fig. 3. The cost function was minimized using MATLAB's nonlinear least squares solver *lsqnonlin* [17] and resulted in values of $\sigma = 0.132$ rad, $\kappa = 0.912$, $u_{\text{low}} = 0.194$, and $u_{\text{high}} = 0.00481$ which are used to plot the three pieces of Eq. (27).

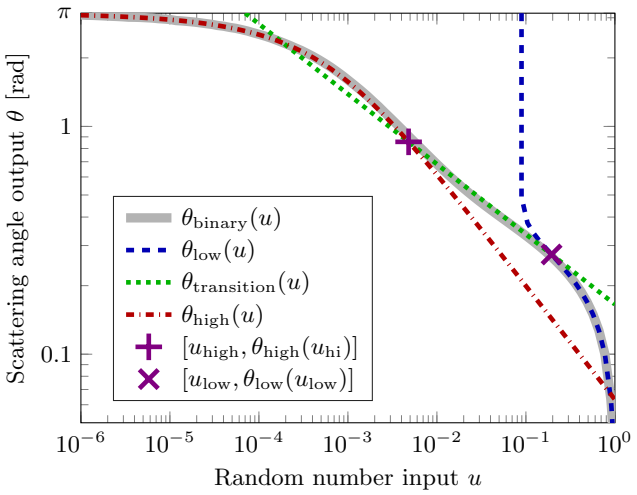

FIG. 3. Comparison of scattering angles produced by the cumulative binary collision approximation with scattering angles produced by the three pieces of Eq. (27).

D. Trends for σ, κ, U_{low}, and U_{high}

To be useful for a plasma simulation, the values of σ, κ, u_{low}, and u_{high} need to be easily approximated for a given pair of a and N. These parameters can be found by repeating the process outlined in Sec. V C for a range over both a and N and then finding fit functions that closely follow the values found.

1. *Low-angle regime*

For low values of a and/or N the peak scattering angle is low ($\sigma \to 0$, $\varsigma \to \infty$) and the values of $\tilde{\sigma} \equiv \frac{\sigma}{a\sqrt{N}}$, κ, u_{low}, and u_{high} have logarithmic dependence on N, and no dependence on a. The functional fits chosen for these four parameters, using the shorthand $\underset{a\to 0}{x} \equiv \lim_{a\to 0}[x(a,N)]$ are

$$\underset{a\to 0}{\tilde{\sigma}} = -K_\sigma^{(1)} \exp\left(-K_\sigma^{(2)} N^{K_\sigma^{(3)}}\right) + K_\sigma^{(4)} \tag{31a}$$

$$\underset{a\to 0}{\kappa} = -K_\kappa^{(1)} \exp\left(-K_\kappa^{(2)} N^{K_\kappa^{(3)}}\right) + 1 \tag{31b}$$

$$\underset{a\to 0}{u_{\text{low}}} = K_{u_{\text{low}}}^{(1)} \exp\left(-K_{u_{\text{low}}}^{(2)} N^{K_{u_{\text{low}}}^{(3)}}\right) \tag{31c}$$

$$\underset{a\to 0}{u_{\text{high}}} = K_{u_{\text{high}}}^{(1)} \exp\left(-K_{u_{\text{high}}}^{(2)} N^{K_{u_{\text{high}}}^{(3)}}\right) \tag{31d}$$

where all values of K are positive. Only values of $N \geq 1000$ are used for finding the best-fit parameters, and so the equations are only to be considered valid in this range. In cases where N is large, M must be small so that computation time (which is approximately $MN \times 10^{-9}$ s per data point) remains reasonable. Numerical data for different values of M are shown alongside plots of Eqs. (31) in Fig. 4. Best-fit values for K were found using again MATLAB's nonlinear least squares solver *lsqnonlin*.

2. *High-angle regime*

When a and/or N are not low, $\tilde{\sigma}$, σ, κ, u_{low}, and u_{high} have dependence on both a and N. The functional fits chosen for extending Eqs. (31) into the high-angle regime

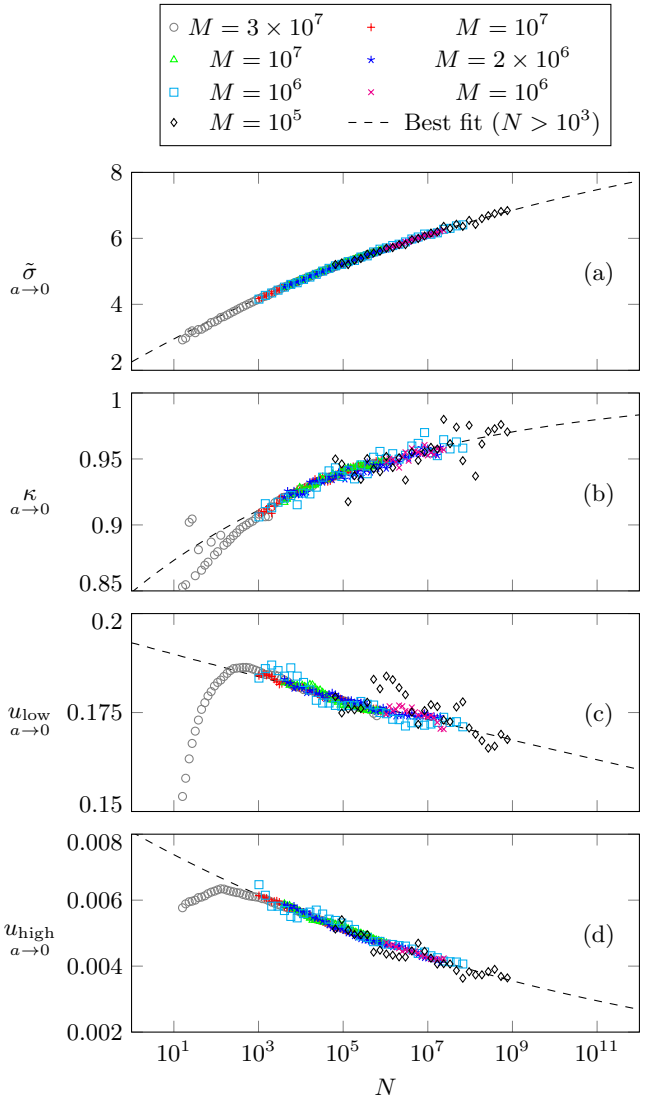

FIG. 4. Values of (a) $\tilde{\sigma}$, (b) κ, (c) u_{low}, and (d) u_{high} from individual numerical experiments performed at varying values of N and M, found by fitting Eqs. (25) and (26) to numerical data produced by Eq. (11). Best-fit curves of Eq. (31) are fit to the data points for $N > 10^3$ only.

are

$$\sigma(a,N) = a\sqrt{N}\underset{a\to 0}{\tilde{\sigma}}\left\{1+\left(\frac{2}{\pi}a\sqrt{N}\underset{a\to 0}{\tilde{\sigma}}\right)^{K_\sigma^{(5)}}\right\}^{\frac{1}{K_\sigma^{(5)}}} \tag{32a}$$

$$\kappa(a,N) = \min\left[1,\ \underset{a\to 0}{\kappa}\exp\left(K_\kappa^{(4)}\sigma^{K_\kappa^{(5)}}\right)\right] \tag{32b}$$

$$u_{\text{low}}(a,N) = \min\left[1,\ \underset{a\to 0}{u_{\text{low}}}\exp\left(-K_{u_{\text{low}}}^{(4)}\sigma^{K_{u_{\text{low}}}^{(5)}}\right)\right] \tag{32c}$$

$$u_{\text{high}}(a,N) = \min\left[1,\ \underset{a\to 0}{u_{\text{high}}}\exp\left(-K_{u_{\text{high}}}^{(4)}\sigma^{K_{u_{\text{high}}}^{(5)}}\right)\right]. \tag{32d}$$

Note that Eqs. (32b), (32c), and (32d) are dependent on Eq. (32a). The best-fit values for the functional fits are:

$$K_\sigma = \begin{bmatrix}1.040\times 10^6\\ 11.76\\ 3.289\times 10^{-3}\\ 10.41\\ 4.17\end{bmatrix}, K_\kappa = \begin{bmatrix}6.776\times 10^7\\ 19.92\\ 3.803\times 10^{-3}\\ 0.4890\\ 2.576\end{bmatrix},$$

$$K_{u_{\text{low}}} = \begin{bmatrix}1.926\times 10^9\\ 20.72\\ 3.164\times 10^{-4}\\ 166.5\\ 6.193\end{bmatrix}, K_{u_{\text{high}}} = \begin{bmatrix}5.307\times 10^7\\ 22.61\\ 1.720\times 10^{-3}\\ 6.248\\ 1.618\end{bmatrix} \tag{33}$$

The fits for these equations are plotted in Fig. 5. The discrepancy in the case of u_{low} is likely due to differences in the implementation of the optimizer between the low-angle and high-angle regimes, but this difference is not large enough to cause a significant change in scattering angles generated by the present model.

VI. COMPARISON OF THE PRESENT METHOD TO PREVIOUS METHODS

Previous methods include the work of Takizuka and Abe [4] and Nanbu [5]. Takizuka and Abe define a scattering angle variance which can be rewritten in terms of the parameters a and N as

$$\langle\delta^2\rangle = 2a^2 N\log\left(\frac{1}{2a}\right). \tag{34}$$

A normally distributed random number, δ, is produced with variance $\langle\delta^2\rangle$ and the scattering angle is calculated as

$$\theta_{\text{Takizuka-Abe}}(\delta) = 2\tan^{-1}(\delta). \tag{35}$$

Nanbu defines an isotropy parameter, s, which may be written in terms of the parameters a and N as

$$s = 4a^2 N\log\left(\frac{1}{2a}\right) \tag{36}$$

and the parameter A is defined in terms of s as

$$\coth A - A^{-1} = \exp(-s). \tag{37}$$

From this value of A, the scattering angle as a function of u is

$$\theta_{\text{Nanbu}}(u) = \cos^{-1}\left\{A^{-1}\log\left[\exp(-A)+2u\sinh(A)\right]\right\}. \tag{38}$$

It is worthwhile to note that Nanbu's parameter A has a similar role to the parameter ς defined in the present work. Results from Nanbu's formulation can be compared to the present model as well as with the results of the cumulative binary collision approximation. The results of this comparison are shown in Fig. 6. The re-

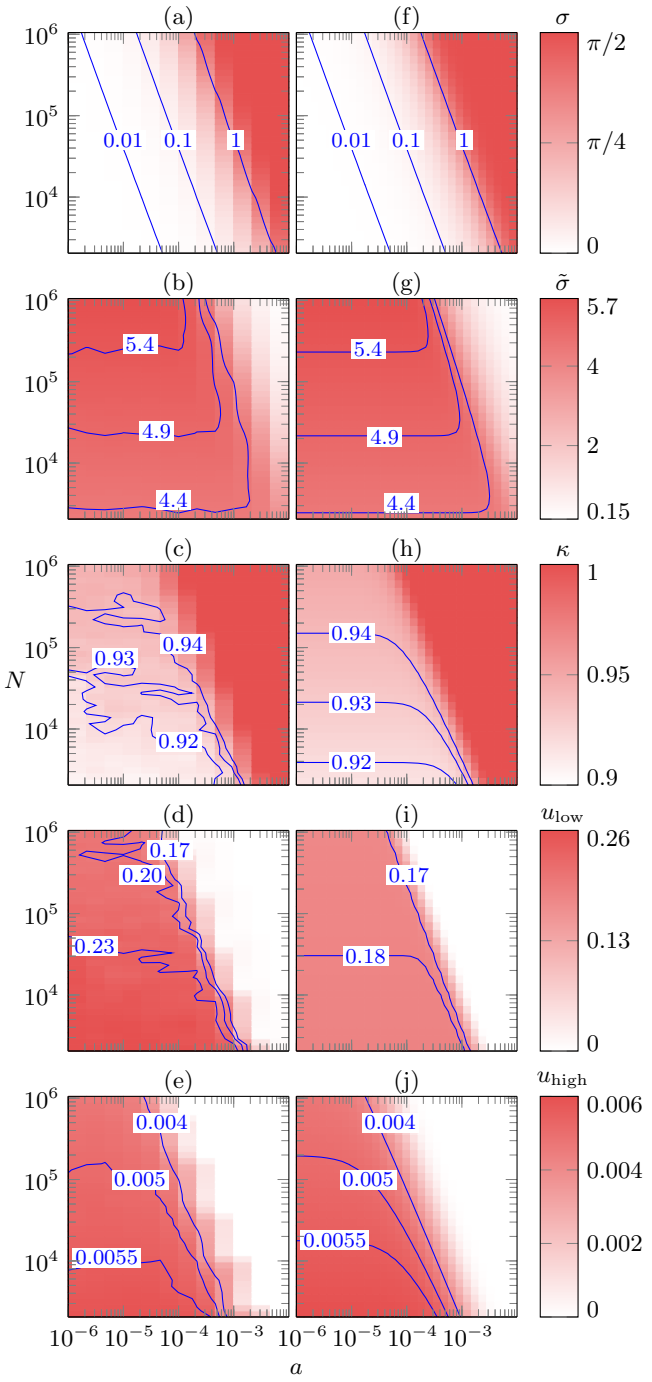

FIG. 5. (a)-(e): Values of σ, $\tilde{\sigma}$, κ, u_{low}, and u_{high} respectively from individual numerical experiments performed at each (a, N) coordinate, found by fitting Eqs. (24) and (26) to numerical data produced by Eq. (8). (f)-(j): Best-fit graphs of Eq. (32) for predicting values of σ, $\tilde{\sigma}$, κ, u_{low}, and u_{high} as a function of a and N. Selected contours of constant value are plotted to aid in comparison.

sults of the Nanbu method are slightly upshifted from the results of the cumulative binary collision approximation, which in turn was shown to be upshifted from the

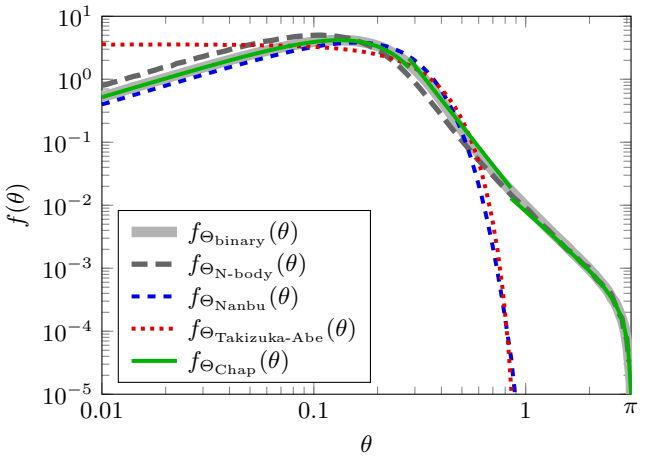

FIG. 6. A comparison of the probability distribution functions for the scattering angle between the cumulative binary collision approximation (Sec. III), the N-body simulation (Sec. IV), the Nanbu method, the Takizuka-Abe method, and the present method (Sec. V)

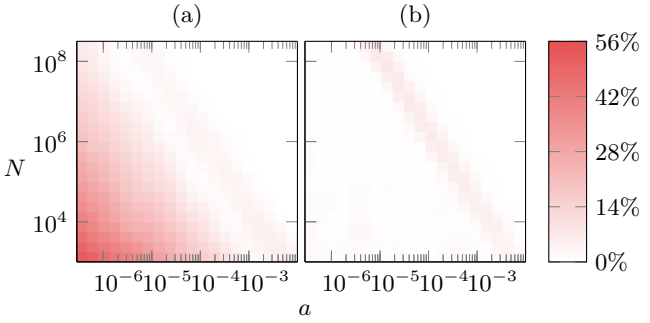

FIG. 7. The percent error of the mean scattering angle as compared to the results of the cumulative binary collision approximation for (a) the Nanbu method and (b) the present method.

N-body simulation of Sec. IV. Most glaringly, however, neither the Takizuka-Abe method nor the Nanbu method recreate the low-probability, high-angle scattering above 0.5 radians seen in both the binary and N-body collision data, as well as the present model. For comparison over a range of a and N, the errors of the average scattering angle relative to the results of the cumulative binary collision approximation for both the Nanbu method as well as the present method are shown in Fig. 7.

VII. IMPLEMENTATION AND COMPARISON TO AN N-BODY SIMULATION

The present collision model is tested by implemention into a 2D3V axisymmetric particle-in-cell (PIC) code previously developed by Chap *et al.* [21]. This simulation was then compared to the results of an N-body simulation of an identical scenario. The scenario chosen is that

of counterstreaming ion beams, to demonstrate the effect of high-angle scatters in a situation that is illustrative of the conditions encountered in inertial electrostatic confinement fusion [11]. Two beam sources are placed facing one another at a distance of 10 mm apart, each producing monoenergetic protons with an initial axial velocity of 10^4 m/s, at a density of $10^{13}\,\mathrm{m}^{-3}$ in an initial beam radius of 0.1 mm. Such a small-scale scenario is chosen so that the N-body simulation can simulate real particles rather than macroparticles. After the simulations reach steady-state, the densities are time-averaged over a long enough duration ($t \approx 0.5\,\mathrm{ms}$) so that the density plot is smooth.

The collision model is implemented into the PIC simulation using the Monte-carlo approach described by Takizuka and Abe [4], in which particles are randomly matched pairwise with other particles in the same simulation cell. For comparison, this PIC simulation was run using the present collision model, Nanbu's collision model, as well as a baseline case of no collision implementation at all. The particles in the PIC simulation are oversampled ($w = 0.1$) to ensure that simulation cells within the beam envelope are well populated.

The N-body simulation for this scenario uses the method of Ref. 14 which in turn is based on Ref. 3 and is similar to the N-body method described in Sec. IV. It uses a particle weighting of unity so that the macroparticle approximation is avoided. The results from these simulations are compared in Fig. 8.

Some inherent differences in these simulations preclude exact agreement. Due to limitations in computational power, the chosen beam radius is quite small compared to the beam density, such that the mean inter-particle spacing ($\approx 0.03\,\mathrm{mm}$) is not small compared to the beam radius, meaning that the beam is not as axially symmetric as the initial conditions may suggest, and may also be the reason that the beam envelope is less sharply defined in the density profile of the N-body simulation as compared to the PIC simulation. Another inherent difference is that the N-body simulation has completely open boundary conditions, which is not feasible within a PIC simulation. To reduce unwanted boundary effects, Dirichlet boundary conditions in the PIC simulation were placed at twice the axial extent ($x = 10\,\mathrm{mm}$) and twice the radial extent ($x = 2\,\mathrm{mm}$) so that the boundaries would not have a significant effect on the beam envelope.

VIII. DISCUSSION OF SMALL IMPACT PARAMETERS

Collision models generally make use of a minimum impact parameter, below which collisions are not considered. In the present work, charged particles are treated as points with no spatial extent, and no minimum impact parameter is assumed. In actuality, the scattering angle is limited by the size and nature of the participating particles. As an example, collisions between protons and Boron-11 in a plasma (referred to as p-^{11}B fusion fuel) are considered under IEC fusion conditions [14]. The following considerations are present in relevant literature concerning the lower limit of impact parameters:

- A fusion event occurs if the impact parameter between any two particles is below the experimentally determined maximum fusion impact parameter.
- The particles may come within a de Broglie wavelength of each other, suggesting that their matter waves have overlapped to such an extent that the point-charge Coulomb force is no longer an accurate representation of the interaction between them. The distance at which this occurs is used in some models as the minimum impact parameter [22, 23].
- The potential energy of a particle pair may exceed the kinetic energy of the particle pair in the center-of-mass frame. The distance between particles at this limit is used as a minimum impact parameter for some collision models [24] though it serves only as a relevant scale and has no immediately obvious physical significance. Many other models use similar scales pertaining to the potential energy of the particle pair [25, 26].

In assessing these conditions, it is assumed that a high cumulative scattering angle results from a single high-angle scatter that makes all low-angle scatters negligible over the time-step, i.e. $U \ll u_{\mathrm{high}}$. The scattering angle for this region is given by Eq. (21). In this limit, the minimum impact parameter experienced by the test particle is the impact parameter that would result in this scattering angle from a binary collision with one field particle:

$$b_{\min}\left(U \ll u_{\mathrm{high}}\right) = \sqrt{\frac{U}{n_\beta v_{\alpha\beta} \tau \pi}}. \tag{39}$$

The distance of closest approach r_0 during a single binary collision as a function of the impact parameter and scattering angle is

$$r_0\left(\theta, b\right) = b\frac{\cos\left(\frac{\theta}{2}\right)}{1-\sin\left(\frac{\theta}{2}\right)}. \tag{40}$$

Combining Eqs. (21), (39), and (40) reveals the minimum of r_0 among all binary collisions, i.e. the minimum of the closest approaches between the test particle and all field particles:

$$r_{\min}\left(U \ll u_{\mathrm{high}}\right) = a b_{\max}\left(1+\sqrt{1+\frac{U}{a^2 N}}\right). \tag{41}$$

A. Fusion event

The maximum impact parameter for a fusion event is $b_{\mathrm{fusion}} = \sqrt{\frac{\sigma_{\mathrm{fusion}}}{\pi}}$, so a randomly generated scattering

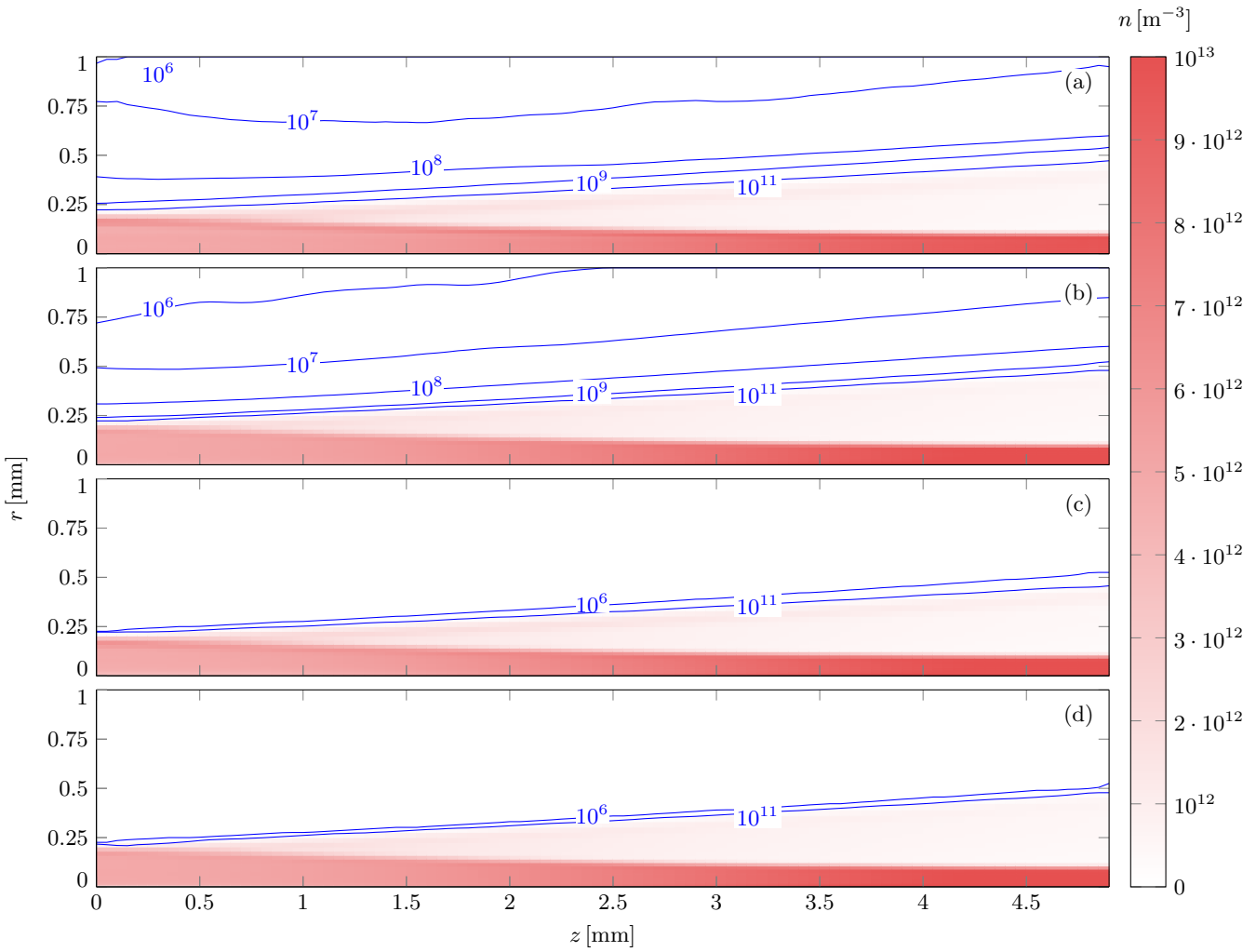

FIG. 8. Time-averaged density for simulations of counterstreaming beams using (a) the N-body method, (b) a particle-in-cell simulation with the present collision model, (c) a particle-in-cell simulation with Nanbu's collision model, and (d) a collisionless particle-in-cell simulation. The plots are axisymmetric about the z-axis and plane-symmetric about the r-axis. In all simulations, the envelope of the beam sourced at $z = 5\,\mathrm{mm}$ is visible as a dark shade and the envelope of the beam sourced at $z = -5\,\mathrm{mm}$ is visible as a light shade. The density resulting from high-angle scatters permeates the remainder of the domain and is displayed using contour lines of constant value. Densities down to $10^6\,\mathrm{m}^{-3}$ are resolved by time-averging the density over 0.5 ms. Densities below $10^6\,\mathrm{m}^{-3}$ are not resolved.

angle that suggests a lower impact parameter than b_{fusion} can be assumed to have resulted in the fusion of the test particle with a field particle. The range of u for which U results in a fusion event is defined as

$$u_{\mathrm{fusion}} \leq n_\beta v_{\alpha\beta} \tau \sigma_{\mathrm{fusion}}. \tag{42}$$

u_{fusion} is equivalent to the probability of the test particle fusing with a field particle during an amount of time τ.

B. de Broglie wavelength

The de Broglie wavelength of a particle is

$$\lambda_{\text{de Broglie}} = \frac{h}{p} \tag{43}$$

where h is the Planck constant and p is the particle momentum. The criterion of interest is if at any time the distance between the test particle and any field particle becomes less than the sum of their de Broglie wavelengths. This criterion is satisfied if and only if the minimum of the distances of closest approach given by Eq. (41) is less than or equal to the sum of the de Broglie wavelengths of the particles:

$$r_{\min}\left(U \ll u_{\mathrm{high}}\right) \leq \lambda_{\text{de Broglie}}. \tag{44}$$

From the difference of the initial kinetic energy and the potential energy at closest approach, the momentum of

the particle pair at closest approach can be found:

$$p = 2\mu_{\alpha\beta}\sqrt{v_{\alpha\beta}^2 - \frac{e^2}{4\pi\epsilon_0\mu_{\alpha\beta}r_{\min}}}. \tag{45}$$

Combining Eqs. (41), (44) and (45), the range of values for which U results in the test particle coming within a distance of any field particle less than or equal to the sum of their de Broglie wavelengths is defined:

$$u_{\text{de Broglie}} \leq a^2 N \left\{ \frac{1}{4}\left[\sqrt{1+\left(\frac{4\pi\epsilon_0 v_{\alpha\beta}h}{q_\alpha q_\beta}\right)^2} - 1\right]^2 - 1 \right\}. \tag{46}$$

C. Potential energy equal to kinetic energy

The potential energy of the particle pair exceeds its kinetic energy when its potential energy at closest approach exceeds half its initial kinetic energy:

$$\frac{q_\alpha q_\beta}{4\pi\epsilon_0 r_{\min}} \geq \frac{1}{4}\mu_{\alpha\beta}v_{\alpha\beta}^2. \tag{47}$$

Combining Eqs. (41) and (47) results in the range of values for which U results in a test particle field particle pair having a higher potential energy than kinetic energy at closest approach:

$$u_{\text{potential}} \leq 8a^2 N. \tag{48}$$

For comparison of u_{fusion}, $u_{\text{de Broglie}}$, and $u_{\text{potential}}$ under p-^{11}B fusion conditions, either species can be assigned as the α species and the other assigned to the β species. The velocities are chosen such that the center-of-mass energy is equal to the resonant center-of-mass peak fusion cross-section that occurs at approximately 148.3 keV [27] where the fusion cross section is approximately $\sigma_{\text{fusion}} = 10^{-29}\,\text{m}^2$. The densities are chosen to be $n_p = n_B = 10^{16}\,\text{m}^{-3}$ with $\tau = 10^{-8}\,\text{s}$. To avoid electron shell effects, Boron nuclei are simulated ($q_\text{B} = 5e$.) The values of u_{fusion}, $u_{\text{de Broglie}}$, and $u_{\text{potential}}$ are plotted in Fig. 9. It is clear that above these limits, high angle scattering beyond that which is predicted by Nanbu's model is present in this particular IEC fusion scenario.

IX. CONCLUSION

A collision model for non-thermal plasma simulation has been formulated based on data obtained by numerical experimentation on the effect of repeated binary collisions on a test particle. The present effort expands on previous efforts by accounting for low-probability, high-angle scatters and by limiting the model input to two parameters: a and N (Eqs. (6) and (2) respectively). From these two parameters, the values σ, κ, u_{low}, and u_{high} are calculated from Eqs. (31) and (32). Finally, the scattering angle is calculated from a random number input using Eq. (27). Numerical experiments show that this model recovers high-angle scatters not seen in previous models, and conforms well to numerical data produced by the cumulative binary collision approximation. Lastly, a significant range of high-angle scatters was shown to be present at impact parameters above commonly defined forms of a minimum impact parameter $b_{\min}$ in a highly non-thermal plasma.

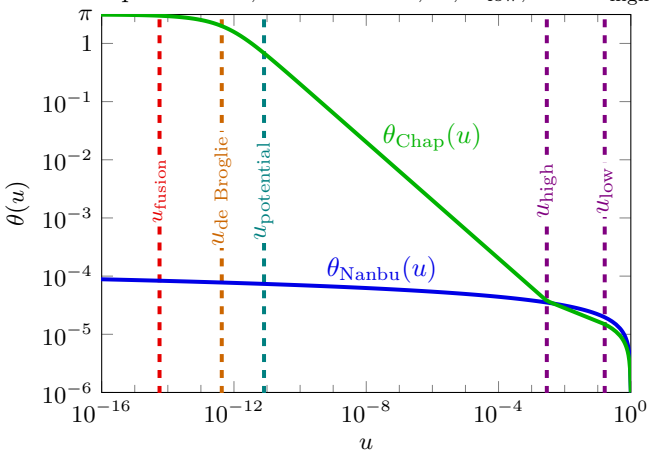

FIG. 9. A comparison of scattering angle probabilities with the probabilities of u_{fusion} (a fusion event), $u_{\text{de Broglie}}$ (significant interaction of matter waves), and $u_{\text{potential}}$ (potential energy exceeding kinetic energy) occuring.

ACKNOWLEDGMENTS

This work is supported by a NASA Space Technology Research Fellowship, grant number NNX13AL44H.

[1] D. Scharfetter and H. Gummel, Electron Devices, IEEE Transactions on **16**, 64 (1969).

[2] C. K. Birdsall and A. B. Langdon, *Plasma physics via computer simulation* (Taylor and Francis, New York, NY,

2005).
[3] S. Aarseth, *Gravitational N-Body Simulations: Tools and Algorithms*, Cambridge Monographs on Mathematical Physics (Cambridge University Press, 2003).
[4] T. Takizuka and H. Abe, Journal of Computational Physics **25**, 205 (1977).
[5] K. Nanbu, Physical Review E **55**, 4642 (1997).
[6] A. M. Dimits, C. Wang, R. Caflisch, B. I. Cohen, and Y. Huang, Journal of Computational Physics **228**, 4881 (2009).
[7] E. Rutherford, Philosophical Magazine Series 6 **21**, 669 (1911).
[8] M. Conte, Nuclear Instruments and Methods in Physics Research Section A: Accelerators, Spectrometers, Detectors and Associated Equipment **228**, 236 (1985).
[9] L. Spitzer, *Physics of Fully Ionized Gases, New York: Interscience (2nd edition), 1962* (Dover Publications, 2013).
[10] D. Wu, X. T. He, W. Yu, and S. Fritzsche, Phys. Rev. E **95**, 023208 (2017).
[11] R. L. Hirsch, Journal of Applied Physics **38**, 4522 (1967).
[12] C. Dietrich, R. Sedwick, and L. Eurice, in *44th AIAA/ASME/SAE/ASEE Joint Propulsion Conference and Exhibit* (Hartford, CT, 2008).
[13] J.-P. Wulfkuehler and M. Tajmar, in *52nd AIAA/SAE/ASEE Joint Propulsion Conference* (American Institute of Aeronautics and Astronautics (AIAA), 2016).
[14] A. M. Chap and R. J. Sedwick, in *51st AIAA/SAE/ASEE Joint Propulsion Conference* (American Institute of Aeronautics and Astronautics (AIAA), 2015).
[15] R. Courant, K. Friedrichs, and H. Lewy, Mathematische Annalen **100**, 32 (1928).
[16] Z. Donkó, Journal of Physics A: Mathematical and Theoretical **42**, 214029 (2009).
[17] MATLAB, *version 9.1 (R2016b)* (The MathWorks Inc., Natick, Massachusetts, 2016).
[18] S. D. Baalrud and J. Daligault, Phys. Rev. Lett. **110**, 235001 (2013).
[19] S. D. Baalrud and J. Daligault, Physics of Plasmas **21**, 055707 (2014).
[20] C. B. Moler, *Numerical Computing with Matlab* (Society for Industrial & Applied Mathematics (SIAM), 2004).
[21] A. M. Chap, A. G. Tarditi, and J. H. Scott, in *50th AIAA/ASME/SAE/ASEE Joint Propulsion Conference* (American Institute of Aeronautics and Astronautics (AIAA), 2014).
[22] Y. Sentoku and A. Kemp, Journal of Computational Physics **227**, 6846 (2008).
[23] A. Robinson, D. Strozzi, J. Davies, L. Gremillet, J. Honrubia, T. Johzaki, R. Kingham, M. Sherlock, and A. Solodov, Nuclear Fusion **54**, 054003 (2014).
[24] R. Fitzpatrick, *Plasma Physics: An Introduction* (CRC Press, Boca Raton, FL, 2014).
[25] M. Keidar and I. Beilis, *Plasma Engineering: Applications from Aerospace to Bio and Nanotechnology* (Academic Press, 2013).
[26] R. Alexandre and C. Villani, Annales de l'Institut Henri Poincare (C) Non Linear Analysis **21**, 61 (2004).
[27] H. W. Becker, C. Rolfs, and H. P. Trautvetter, Zeitschrift für Physik A Atomic Nuclei **327**, 341 (1987).